Resonant electron capture by B-like ions at low energies

H. H. Ramadan* and Y. Hahn
Department of Physics, University of Connecticut, Storrs, Connecticut 06268
(Received 1 August 1988)

Dielectronic recombination cross sections and rates are estimated for ions of the B isoelectronic sequence, (C^{1+}, O^{3+}, Ar^{13+}, and Fe^{21+}), in which the $2s \rightarrow 2p$ excitation is involved during the initial capture. A complete set of rates is then generated for all ions by extrapolation. The rates increase rapidly with nuclear core charge Z_c, reaching a maximum at $Z_c \sim 10-12$. A surprisingly smooth variation within the isonuclear sequence around the B-like ions is observed.

I. INTRODUCTION

Resonant processes in electron-ion collisions have received increasing attention in recent years, both experimentally and theoretically, because they play often a dominant role in collisional excitation, ionization, and capture. Their cross sections and rate coefficients are important input data in modeling astrophysical and laboratory plasmas. Furthermore, various resonant amplitudes are interrelated,[1] so that a unified treatment of these processes can be given and their data correlated. As a continuation of the study of the resonant capture process [dielectronic recombination (DR)] in electron-ion collisions,[2] we examine the DR involving B-like target ions at low energies where the $\Delta n_t = 0$ transitions are dominant. In particular, we will explicitly treat the ions C^{1+}, O^{3+}, Ar^{13+}, and Fe^{21+} for the purpose of generating by extrapolation a complete set of DR rates for all ions of the B sequence. The process of interest involves an initial excitation capture in going from initial state i to intermediate state d,

$$1s^2 2s^2 2p + l_c e_c \rightarrow 1s^2 2s 2p^2 nl \quad (2s \rightarrow 2p, \quad \Delta n_t = 0, \quad n_t = 2), \qquad (1)$$

which is followed by a radiative decay of the intermediate state d to final state f,

$$1s^2 2s 2p^2 nl \rightarrow 1s^2 2s^2 2pnl + \gamma(2p \rightarrow 2s) \rightarrow 1s^2 2s 2p^2 n'l' + \gamma(nl \rightarrow n'l'). \qquad (2)$$

The radiative transitions involving $nl \rightarrow n'l' = (l \pm 1) + \gamma'$ are much slower for light ions, but are important for heavier targets.

The C^{1+} system, with the nuclear charge $Z_c = 6$ and the number of electrons $N = 5$ in the target ion, was studied earlier experimentally[3] and theoretically,[4] but possibly strong field contamination made it difficult to make a meaningful comparison. More recently, a merged-beam experiment with N^{2+}, O^{3+}, and F^{4+} was performed by Dittner *et al.*,[5] in which the term splittings of the core states $(1s^2 2s 2p^2) L_t S_t$ were clearly separated (in O^{3+} and F^{4+}) and where $L_t S_t \rightarrow L_t' S_t'$ Auger transitions are important. Obviously, this provides more detailed information on the reaction mechanism in terms of the resonance positions and relative peak ratios. Because of the small excitation energies involved in (1), the capture takes place to high Rydberg states (HRS's) which are sensitive to an external electric field in the interaction region.[6] Therefore the rates presented here, obtained in the zero-field zero-density limit, will eventually be modified by external perturbations. Such modifications can be L_t dependent; this problem is being treated in detail and will be reported on elsewhere.

II. THEORY

There are several possible modes of excitations when projectile electrons collide with a B-like target ion: for the initial state $i = 1s^2 2s^2 2p$, the $2p$ electron may be excited to $n_a \geq 3$ ($i + e_c l_c \rightarrow 1s^2 2s^2 n_a l_a nl$), the $2s$ electron to either $2p$ or to states with $n_a \geq 3$, and finally the $1s$ electron excitation. The excitation energies for the different excitation modes may generally be grouped into well-separated energy regions. In the following, we limit the projectile energy e_c to the low-energy region such that only the $2s \rightarrow 2p$ excitation in (1) is energetically allowed. This mode ($\Delta n_t = 0$) is often dominant for light ions and at low temperatures, and is accompanied by the projectile electron being captured to a high Rydberg state.

As in previous work,[2] we employ the single-configuration, nonrelativistic Hartree-Fock wave functions and LS coupling in evaluating the necessary amplitudes. (The relativistic corrections are expected to be $\sim 5-10\%$ for Ar^{13+} and Fe^{21+}). Thus we have for the intermediate state d in (1)

$$|d\rangle = |([1s^2 2s, 2p^2(L_a S_a)] L_t S_t, nl) LS\rangle \quad (L_a = L_t), \qquad (3a)$$

and the initial ground state

$$|i\rangle = |((1s^2 2s^2 2p) L_t S_t, e_c l_c) LS\rangle \equiv i_1 \quad \text{with} \quad L_t = 1, \quad S_t = \tfrac{1}{2}. \qquad (3b)$$

The metastable initial state

$$|i'\rangle = |([1s^2 2s 2p^2(L_a S_a)](L_t=1, S_t=\tfrac{3}{2}), e_c' l_c')LS\rangle \quad (3c)$$

may also be present in actual experiment;[5] the target ions can have a large mixture of metastable states, depending on the ways by which the ions are produced experimentally.

The DR cross section σ^{DR} is defined[2] by

$$\sigma^{\mathrm{DR}}(i, e_c l_c \to d \to f) = \frac{4\pi\tau_0}{e_c(\mathcal{R})} V_a(i, l_c \to d)\omega(d \to f)\hat{\delta}(e_c, E_d)(\pi a_0^2) , \quad (4)$$

where

$$V_a(i, l_c \to d) = \frac{g_d}{2g_i} A_a(d \to i)$$

is the radiationless excitation-capture probability in sec^{-1} and $\mathcal{R}$ is the hydrogen Rydberg. In LS coupling,

$$g_d = \hat{L}\hat{S} \quad \text{with } \hat{L} \equiv 2L+1, \text{ etc. and } g_i = 6 ,$$

$$\omega(d \to f) = \frac{A_r(d \to f)}{\Gamma(d)} ,$$

$$\hat{\delta}(e_c, E_d) = \left[\frac{\Gamma(d)}{2\pi}\right] \frac{1}{(E_i + e_c - E_d)^2 + \dfrac{\Gamma(d)^2}{4}} ,$$

$$\int \hat{\delta}\, de_c = 1 .$$

[$\omega(d \to f)$ represents the partial fluorescence yield.] The Lorentzian factor $\hat{\delta}$ in (4) contains the resonance condition $e_c = E_d - E_i$, where E_d is the intermediate-state energy and E_i is the initial target-state energy. The total decay width of the intermediate state d is given by

$$\Gamma(d) = \sum_{i'} A_a(d \to i') + \sum_{f'} A_r(d \to f') \equiv \Gamma_a(d) + \Gamma_r(d) ,$$

and similarly for the total fluorescence yield $\omega(d) = \Gamma_r'/\Gamma$, where Γ_r' involves a summation over the Auger-stable final states reachable by radiative decay. The basic components in (4) are therefore the radiative and Auger transition probabilities, A_r and A_a, respectively.

For the transition (1), we have, from (3a) and (3b),

$$A_a(d \to i) = 6\hat{l}\hat{l}_c^2\hat{L}_t\hat{S}_t\hat{S}_a \begin{Bmatrix} l & L_t & L \\ 1 & l_c & 1 \end{Bmatrix}^2 \left| \sum_{S''=0,1} \hat{S}'' \begin{Bmatrix} \frac{1}{2} & S_t & S'' \\ \frac{1}{2} & \frac{1}{2} & S_a \end{Bmatrix} \begin{Bmatrix} \frac{1}{2} & S_t & S'' \\ \frac{1}{2} & \frac{1}{2} & S \end{Bmatrix} I(l_c, S'') \right|^2 , \quad (5)$$

where

$$I(L_{ab}, S_{ab}) = \sum_K R_K(l_s l_c; l_a l_b) \begin{bmatrix} l_s & K & l_a \\ 0 & 0 & 0 \end{bmatrix} \begin{bmatrix} l_c & K & l_b \\ 0 & 0 & 0 \end{bmatrix} \begin{Bmatrix} l_s & l_a & K \\ I_b & I_c & L_{ab} \end{Bmatrix}$$
$$+ (-)^{L_{ab} - S_{ab}} \sum_{K'} R_{K'}(l_s l_c; l_b l_a) \begin{bmatrix} l_s & K' & l_b \\ 0 & 0 & 0 \end{bmatrix} \begin{bmatrix} l_c & K' & l_a \\ 0 & 0 & 0 \end{bmatrix} \begin{Bmatrix} l_s & l_b & K' \\ l_a & l_c & L_{ab} \end{Bmatrix} ,$$

and

$$R_K(l_s l_c; l_a l_b) = \int_0^\infty \int_0^\infty dr_1 dr_2 r_1^2 r_2^2 \psi_s(r_1)\psi_c(r_2) \frac{r_<^K}{r_>^{K+1}} \psi_a(r_1)\psi_b(r_2) ,$$

$$\psi_c(r_2) \underset{r_2 \to \infty}{\sim} \left[\frac{2}{\pi k_c}\right]^{1/2} \frac{1}{r_2} \sin\left[k_c r_2 + \frac{Z}{k_c}\ln(2k_c r_2) - \frac{l_c\pi}{2} + \delta_{l_c} + \sigma_{l_c}\right] .$$

[Formula (5) is a factor of 2 larger than that given earlier.[4]] Similar formulas are given for the additional Auger channels which may be available in some appropriate energy regions,

$(L_t, S_t) + nl \to (L_t', S_t') + e_c' l_c'$,

$(1, \frac{1}{2}) \to i_1$, i_2, i_3, and i_4 ,

$(0, \frac{1}{2}) \to i_1$, i_2, and i_3 ,

$(2, \frac{1}{2}) \to i_1$ and i_2 ,

$(1, \frac{3}{2}) \to i_1$,

where $i_1 = i$, $i_2 = (L_t' = 1, S_t' = \frac{3}{2})$, $i_3 = (2, \frac{1}{2})$, and $i_4 = (0, \frac{1}{2})$. These are consistent with energy and angular momentum conservations.

On the other hand, there are three possible radiative decay modes:

$$A_r(d\to f_1=2s^2 2pnl)=\hat{S}_a\,A_r^{(0)}(2p\to 2s)\ , \tag{6a}$$

$$A_r(d\to f_2=2s^2 2p^2)=2\,A_r^{(0)}(nl\to 2s)\ , \tag{6b}$$

$$A_r(d\to f_3=2s2p^3)=3\hat{l}\hat{S}_t\,A_r^{(0)}(nl\to 2p)\sum_{S',L'}\hat{S}'\hat{L}'\begin{Bmatrix} L_a & 1 & L' \\ 1 & L & l \end{Bmatrix}^2\begin{Bmatrix} \frac{1}{2} & S_a & S_t \\ \frac{1}{2} & S & S' \end{Bmatrix}^2 |G_{L_aS_a}^{L'S'}|^2\ , \tag{6c}$$

where G is the fractional parantage coefficients for the $2p^3$ state as given, for example, in Ref. 7, and the single-electron radiative probability

$$A_r^{(0)}(l_1\to l_2)=\frac{\alpha_0^3}{6\tau_0}\left[\frac{\hbar\omega}{\mathcal{R}}\right]^3\frac{l_>}{\hat{l}_1}R_1^2(l_1\to l_2)\ ,$$

where $I_2=I_1\pm 1$ and $I_>$ equals the larger of I_1 and I_2, and

$$R_1=\int_0^\infty r^3 dr\,\psi_{l_i}(r)\psi_{l_2}(r)\ ,$$

with $\alpha_0=\frac{1}{137}$, $\tau_0=2.42\times 10^{-17}$ sec.

As will be discussed in Sec. III, (6a) is the dominant mode for the low-Z ions, while (6b) and (6c) become more important at higher Z. The DR rates are given by

$$\alpha^{\rm DR}(i,l_c\to d\to f)\equiv\langle v_c\sigma^{\rm DR}(i,l_c\to d\to f)\rangle = \left[\frac{4\pi\mathcal{R}}{K_BT_e}\right]^{3/2}V_a(i\to d)\omega(d\to f)\times e^{-e_c/K_BT_e}\ ,$$

where K_BT_e is the electron temperature of a plasma which is assumed to be in local thermal equilibrium.

Since the excitation energies involved in (1) are relatively small, the energy-conserving resonant transition, as described by V_a, requires a capture to HRS with large n. In order to estimate the total cross section, the low-n contributions $n_g\le n\lesssim n_s$ are calculated explicitly, where the last Auger channels open at e_c corresponding to $n=n_s=9$, 13, 20, and 23 and the lowest n allowed by energy conservation are $n=n_g=3$, 5, 12, and 12, respectively, for C^{1+}, O^{3+}, Ar^{13+}, and Fe^{21+}. The individual A_a and A_r are then scaled in n for $n\gtrsim n_s$ (and $n_s\gtrsim 2l$) as

$$A_a\sim\frac{f}{n^3}\ ,\qquad A_r(d\to f_1)\sim a\ ,\qquad A_r(d\to f_2)+A_r(d\to f_3)\sim\frac{b}{n^3}\ , \tag{7}$$

where f, a, and b are some fitted constants. These forms are then substituted into the cross section and the rate formulas,[2] for each fixed l, and the resulting n-dependent expressions are used to estimate the high-n contributions.

The high-l contribution ($l\ge 5$) is very important and must be carefully estimated. The maximum l, $l_{\rm max}$, can be as high as 10 for heavy ions, where $l_{\rm max}$ is approximately defined as that l at which the contribution to $\sigma^{\rm DR}$ is reduced to roughly $\frac{1}{3}$ of the peak value. Usually, the peak for a given n occurs at $l\sim 3$–5. Numerical evaluation of the matrix elements involving high-l orbitals is difficult, and we follow the procedure developed earlier;[2] for A_r ($nl\to n'l'$), we use the simple hydrogenic form for the radial wave functions, as given in Ref. 7. This is reasonable for high-Z ions where such A_r's are important, while for low Z, the $nl\to n'l'$ radiative contribution is small. On the other hand, for A_a, the radial integrals are simplified using the Bethe approximation,[2] as

$$R_1(ab|sc)\sim\int_0^\infty r_2^2 dr_2\psi_b(r_2)\psi_c(r_2)/r_2^2\times\int_0^\infty r_1^3 dr_1\psi_a(r_1)\psi_s(r_1) \equiv I_1I_2\ ,$$

where the second integral is the dipole matrix element as in $A_r^{(0)}$. The first integral may be recast into a dipole form[8] as ($b=nl$, $K_c=k_ca_0/Z$)

$$I_1=\frac{n^2}{4}\left[\frac{1}{n^2}+K_c^2\right]^2 Zg(nl;k_cl_c)\ ,$$

with

$$g(nl;k_cl_c)\equiv\frac{Z^2}{n^2}\int_0^\infty dr\,r^3\psi_b(r)\psi_c(r)\ .$$

The g integral can be evaluated in analytic form in terms of hypergeometric functions.

The total cross section for the ($i\to d$) transition is then given by

$$\sigma^{\rm DR}(i,d)=\sum_f\sum_{l_c}\sigma^{\rm DR}(i,l_c\to d\to f) \tag{8}$$

and similarly for the total DR rates $\alpha^{\rm DR}(i,d)$. As n becomes large, the intermediate states d become nearly degenerate both in n and l. In order to summarize the cross sections and rates it is convenient to define[2] an energy-averaged $\sigma^{\rm DR}$, as

$$\bar{\sigma}^{\rm DR}\equiv\frac{1}{\Delta e_c}\int_{e_c-\Delta e_c/2}^{e_c+\Delta e_c/2}\sigma^{\rm DR}(e_c')de_c'\ , \tag{9}$$

where Δe_c is a small energy bin, chosen arbitrarily.

Finally, we have for the total rates

$$\alpha_{\rm tot}^{\rm DR}(i)=\sum_d\alpha^{\rm DR}(i,d)$$

and cross-section sums $\sum(i)\equiv\sum_d\bar{\sigma}^{\rm DR}(i,d)$, where the d sum includes both sums over the quantum numbers

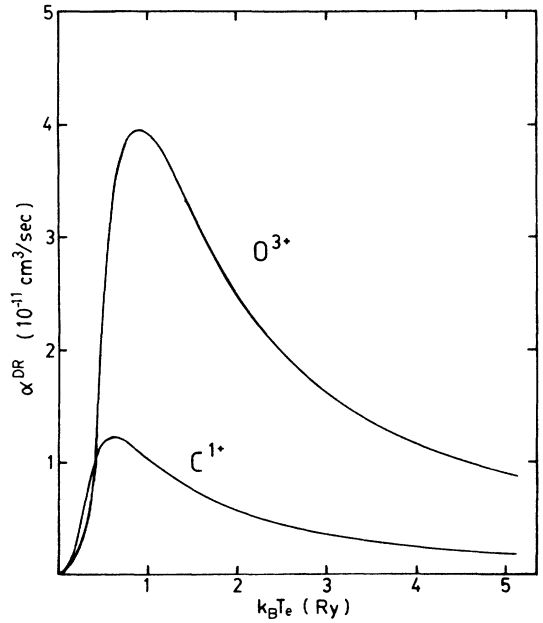

FIG. 1. α^{DR} vs (K_BT_e) for C^{1+} and O^{3+}, in units of 10^{-11} cm^3 sec^{-1}, and temperature in Ry.

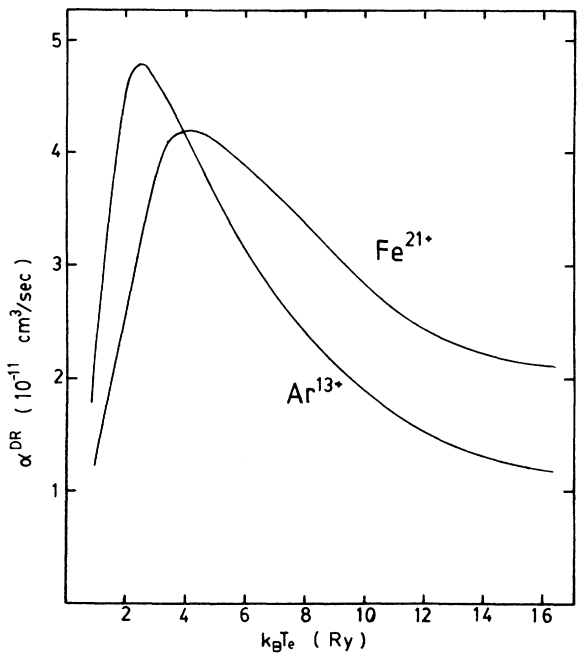

FIG. 2. α^{DR} vs (K_BT_e) for Ar^{13+} and Fe^{21+}, in units of 10^{-11} cm^3 sec^{-1}, and temperature in Ry.

$(L_aS_aL_tS_tLS)$ and also over (nl). The n sum is carried out using the scaling behavior (7) for Γ_a and Γ_r. A convenient formula was given in Ref. 2 for summing the contribution of all $n \geq n_m$ for some n_m. (It was found that, for $n_m \leq 10$, the extrapolation formula given in Ref. 2 can overestimate the contribution by as much as a factor of 2 at some temperatures, because of the variation in e_c which was taken to be that constant corresponding to $n = n_m$. An improved formula is given in the Appendix.) Since the Auger channels i_1, i_2, i_3, and i_4 open up at different threshold energies, extreme caution is required in the summation over n; that is, the n sum using (7) should be carried out only for those n values $n \geq n_s$ where all the energetically allowed Auger channels are open.

III. RESULTS

Cross sections and rate coefficients for the four ions, C^{1+}, O^{3+}, Ar^{13+}, and Fe^{21+} are calculated using the MATRIX code, supplemented by the RCN/RCG code[9] for a more accurate determination of transition energies and transition probabilities in a selected set of cases. As in previous work, one of the crucial steps in treating the process (1) for the $\Delta n_t = 0$ mode is to evaluate all the relevant transition energies properly, since the nonrelativistic, single-configuration Hartree-Fock (HF) program usually does not give accurate enough transition energies, so that separate determination of these energies has to be made, either using a more refined code or referring to experimental data. We used in our calculations the tabulated excitation energies obtained from Ref. 10. These are summarized in Table I with the radiative transition probabilities $A_r(2p \rightarrow 2s)$ for all four ions. The second important step is the estimation of HRS contributions. In particular, the high-l contributions are carefully evaluated following the procedure outlined in Sec. II, and the maximum l_{max} values are determined for each series by explicit calculation. As expected, l_{max} increases with Z. (The

TABLE I. Energies of all the terms of the intermediate-state configuration $1s^22s2p^2$ relative to the $(1s^22s^22p)^2\bar{P}$ target ground state, for C^{1+}, O^{3+}, Ar^{13+}, and Fe^{21+} (Ref. 9), in Ry. The radiative transition probabilities $A_r(2p \rightarrow 2s)$ are also given in sec^{-1}. The powers of 10 are given in square brackets.

$1s^22s2p^2$	C^{1+}	O^{3+}	Ar^{13+}	Fe^{21+}
^2P	1.01	1.65	4.91	8.68
^2S	0.880	1.50	4.59	7.57
^2D	0.683	1.16	3.64	6.60
^4P	0.392	0.652	1.77	3.99
$^2\bar{P}$	0.0	0.0	0.0	0.0
$A_r(^2P)$	0.592[+10]	0.105[+11]	0.366[+11]	0.921[+11]
$A_r(^2S)$	0.131[+10]	0.263[+10]	0.103[+11]	0.204[+11]
$A_r(^2D)$	0.612[+9]	0.121[+10]	0.520[+10]	0.131[+11]

TABLE II. Values of $\bar{\sigma}^{DR}$ vs e_c (Ry) for the excited states ^2S, ^2P, ^2D, and ^4P of C^{1+}. Units of σ^{DR} are 10^{-20} cm^2 and $\Delta e_c = 0.005$ Ry. A large peak in the last bin for the ^4P state is absent because $A_r(2p \rightarrow 2s)$ is forbidden in this case so that all the A_a and A_r decay as n^{-3}.

^4P		^2D		^2S		^2P	
e_c (Ry)	$\bar{\sigma}^{DR}$	e_c (Ry)	$\bar{\sigma}^{DR}$	e_c (Ry)	$\bar{\sigma}^{DR}$	e_c (Ry)	$\bar{\sigma}^{DR}$
0.275	2.48	0.565	21.5	0.760	1.83	0.890	38.8
0.325	0.890	0.615	18.6	0.805	0.410	0.895	18.1
0.345	0.430	0.635	11.3	0.810	1.47	0.940	35.3
0.360	0.240	0.640	6.09	0.830	1.81	0.945	12.8
0.365	0.150	0.645	1.34	0.840	0.460	0.960	33.3
0.370	0.100	0.650	18.1	0.845	1.38	0.970	9.38
0.375	0.120	0.655	12.2	0.850	2.05	0.975	31.7
0.380	0.130	0.660	23.3	0.855	1.81	0.980	37.6
0.385	0.070	0.665	27.9	0.860	4.64	0.985	29.3
		0.670	122.0	0.865	7.29	0.990	64.3
		0.675	688.0	0.870	113.0	0.995	122.0
						1.000	933.0
	4.61		950.0		136.0		1366.0

TABLE III. Values of $\bar{\sigma}^{DR}$ vs e_c (Ry) for the excited states ^2S, ^2P, ^2D, and ^4P of O^{3+}. Units of σ^{DR} are 10^{-20} cm^2 and $\Delta e_c = 0.01$ Ry.

^4P		^2D		^2S		^2P	
e_c (Ry)	$\bar{\sigma}^{DR}$	e_c (Ry)	$\bar{\sigma}^{DR}$	e_c (Ry)	$\bar{\sigma}^{DR}$	e_c (Ry)	$\bar{\sigma}^{DR}$
0.25	1.15	0.76	1.24	1.10	0.281	1.25	2.22
0.27	0.380	0.77	2.41	1.11	0.379	1.26	1.29
0.28	12.1	0.79	16.3	1.13	4.61	1.27	8.30
0.29	2.60	0.87	0.880	1.21	0.141	1.28	31.2
0.36	0.465	0.88	1.71	1.22	0.126	1.36	2.00
0.38	0.157	0.90	19.0	1.24	4.09	1.37	1.17
0.39	5.08	0.93	0.721	1.28	0.126	1.38	7.28
0.40	1.09	0.95	1.40	1.29	0.114	1.39	40.3
0.43	0.248	0.96	3.17	1.30	0.680	1.42	1.88
0.44	0.0842	0.97	18.3	1.31	3.95	1.44	1.10
0.46	3.33	0.98	0.637	1.32	0.118	1.45	6.76
0.47	0.151	0.99	1.23	1.33	0.108	1.46	41.2
0.49	0.0515	1.01	22.4	1.35	4.75	1.47	1.81
0.50	1.78	1.02	1.14	1.36	0.104	1.48	1.07
0.51	0.362	1.03	0.557	1.37	0.109	1.49	7.95
0.52	0.104	1.04	23.2	1.38	4.77	1.50	40.2
0.53	1.27	1.06	23.1	1.40	4.66	1.51	0.941
0.54	0.159	1.07	3.69	1.41	0.841	1.52	7.75
0.55	0.838	1.08	22.4	1.42	4.10	1.53	41.2
0.56	0.198	1.09	23.3	1.43	5.22	1.54	7.59
0.57	0.761	1.10	28.5	1.44	4.87	1.55	39.4
0.58	0.571	1.11	52.3	1.45	10.5	1.56	18.9
0.59	0.447	1.12	125.0	1.46	21.7	1.57	37.0
0.60	0.580	1.13	133.0	1.47	26.0	1.58	44.7
0.61	0.580	1.14	220.0	1.48	41.0	1.59	90.0
0.62	0.419	1.15	775.0	1.49	151.0	1.60	176.0
0.63	0.473					1.61	157.0
0.64	0.375					1.62	222.0
						1.63	976.0
	35.8		1521.0		294.0		2014.0

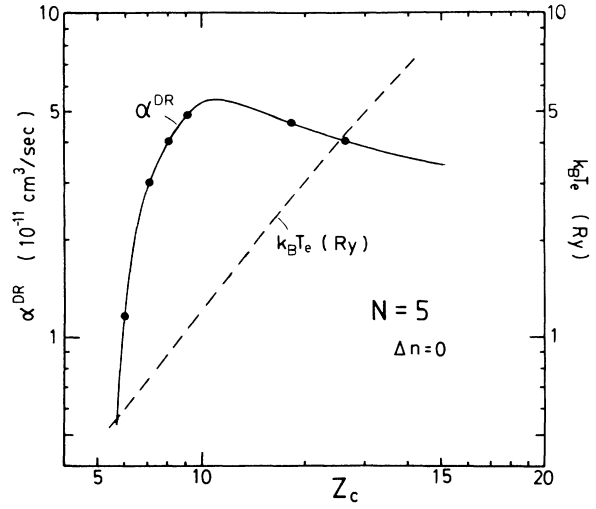

FIG. 3. α^{DR} vs (Z_c) for B-like ions C^{1+}, N^{2+}, O^{3+}, F^{4+}, Ar^{13+}, and Fe^{21+}, in units of 10^{-11} cm^3 sec^{-1}. The maximum rates were chosen in this plot, rather than the rates at scaled temperatures. The corresponding electron temperatures T_e at which the rates are maximum are also shown.

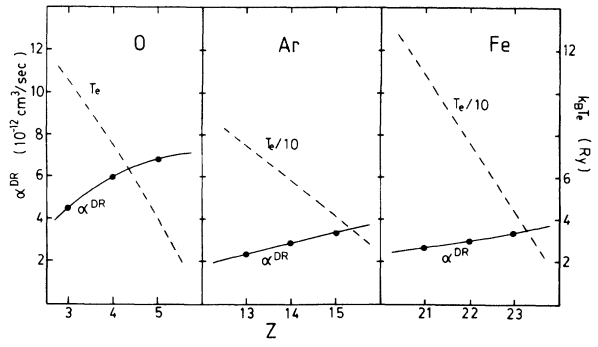

FIG. 4. α^{DR} vs (Z_c) for the isonuclear sequences with $N=3$, 4, and 5 for the ions O, Ar, and Fe. The rates are given in units of 10^{-12} cm^3/sec (solid curve). The temperature k_BT_e (dashed curve) for O is in Ry, and for Ar and Fe is in units of 10 Ry.

value of l_{max} is used[11] in estimating the effect of possible field enhancement of σ^{DR}.)

For light ions and low n, we have $A_a \gg A_r(d\rightarrow f_1)$, and $A_r(d\rightarrow f_1) \gg A_r(d\rightarrow f_2, f_3)$. Therefore, to a good approximation,

$$\sigma^{DR} \sim \frac{g_d}{2g_i} A_r(d\rightarrow f_1)\frac{1}{e_c} ,$$

which is nearly independent of n.

The cross sections σ^{DR}, together with the incident electron energies e_c, are tabulated in Tables II–V for each ion, using the energy bin $\Delta e_c = 0.005$ Ry for C^{1+}, 0.01 Ry for O^{3+}, 0.05 Ry for Ar^{13+}, and 0.1 Ry for Fe^{21+}. They can readily be used to convert σ^{DR} into the corresponding DR rate coefficients.[2] The total rates are shown in Figs. 1 and 2, for (C^{1+} and O^{3+}) and (Ar^{13+} and Fe^{21+}), respectively, while the Z_c dependence is summarized in Fig. 3 for the maximum α^{DR}_{tot}.

The final summary is given in Table VI, where l_{max} are also given. The maximum field-enhancement factor r_F may be estimated by a simple state counting.[2] Explicitly, r_F is given by

TABLE IV. Values of $\bar{\sigma}^{DR}$ vs e_c (Ry) for the excited states ^2S, ^2P, ^2D, and ^4P of Ar^{13+}. Units of σ^{DR} are 10^{-20} cm^2 and $\Delta e_c = 0.05$ Ry.

^4P		^2D		^2S		^2P	
e_c (Ry)	$\bar{\sigma}^{DR}$	e_c (Ry)	$\bar{\sigma}^{DR}$	e_c (Ry)	$\bar{\sigma}^{DR}$	e_c (Ry)	$\bar{\sigma}^{DR}$
0.45	28.4	2.30	24.0	3.25	5.20	3.55	17.3
0.60	16.3	2.40	10.1	3.40	4.56	3.65	12.2
0.75	10.8	2.50	10.3	3.55	4.14	3.75	27.6
0.85	7.65	2.60	18.0	3.60	1.91	3.85	15.2
0.95	5.72	2.70	16.1	3.70	2.40	3.90	10.5
1.00	4.43	2.80	14.8	3.75	1.76	4.00	37.3
1.10	3.52	2.90	14.0	3.85	2.84	4.10	21.6
1.15	2.86	2.95	12.6	3.90	2.70	4.25	16.5
1.20	2.36	3.00	12.0	3.95	2.40	4.25	23.2
1.25	3.60	3.05	11.2	4.00	3.32	4.30	17.6
1.30	2.66	3.10	19.7	4.05	2.82	4.35	18.0
1.35	2.01	3.15	18.3	4.10	4.33	4.40	21.9
1.40	2.81	3.20	21.8	4.15	3.85	4.45	40.2
1.45	1.82	3.25	25.6	4.20	5.90	4.50	35.3
1.50	2.52	3.30	30.4	4.25	8.12	4.55	40.5
1.55	1.76	3.35	58.8	4.30	10.5	4.60	66.8
1.60	1.86	3.40	99.2	4.35	20.1	4.65	74.2
		3.45	263.0	4.40	45.0	4.70	93.7
						4.75	168.0
	101.0		680.0		132.0		758.0

TABLE V. Values of $\bar{\sigma}^{DR}$ vs e_c (Ry) for the excited states ^2S, ^2P, ^2D, and ^4P of Fe^{21+}. Units of σ^{DR} are 10^{-20} cm^2 and $\Delta e_c = 0.1$ Ry.

^4P		^2D		^2S		^2P	
e_c (Ry)	$\bar{\sigma}^{DR}$	e_c (Ry)	$\bar{\sigma}^{DR}$	e_c (Ry)	$\bar{\sigma}^{DR}$	e_c (Ry)	$\bar{\sigma}^{DR}$
0.5	3.23	3.0	43.3	4.0	0.198	5.2	34.9
0.6	15.3	3.1	1.29	4.1	5.53	5.7	0.669
1.0	8.44	3.6	31.9	4.6	2.08	5.8	28.3
1.3	0.845	4.0	13.5	4.7	2.37	6.2	16.4
1.4	4.23	4.1	11.2	5.1	3.65	6.3	8.42
1.6	0.569	4.4	19.6	5.4	1.73	6.5	0.484
1.7	2.86	4.5	0.480	5.5	1.40	6.6	21.4
1.9	2.48	4.7	17.0	5.7	1.61	6.8	0.432
2.1	1.88	4.9	15.5	5.8	1.14	6.9	19.2
2.2	0.243	5.0	0.316	5.9	0.0585	7.1	17.9
2.3	1.23	5.1	12.9	6.0	2.40	7.3	16.4
2.4	1.18	5.2	0.266	6.1	0.0507	7.4	0.342
2.5	0.970	5.3	11.8	6.2	2.19	7.5	15.0
2.6	0.800	5.4	10.6	6.3	1.34	7.6	14.2
2.7	0.680	5.5	7.04	6.4	0.760	7.7	8.85
2.8	0.650	5.6	9.58	6.5	1.87	7.8	12.7
2.9	0.910	5.7	11.3	6.6	1.79	7.9	16.0
3.0	0.700	5.8	8.18	6.7	1.68	8.0	11.4
3.1	0.600	5.9	13.2	6.8	1.62	8.1	16.9
3.2	0.780	6.0	13.8	6.9	2.49	8.2	18.9
3.3	0.630	6.1	18.3	7.0	2.72	8.3	24.6
3.4	0.660	6.2	20.2	7.1	2.52	8.4	26.2
3.5	0.620	6.3	23.2	7.2	3.37	8.5	31.3
3.6	0.510	6.4	34.4	7.3	3.95	8.6	43.0
		6.5	52.8	7.4	5.23	8.7	60.7
		6.6	87.4	7.5	6.97	8.8	84.1
				7.6	21.5		
				7.7	6.85		
	51.0		489.0		89.1		549.0

$$r_F \sim \frac{n_F}{(l_{\max}+1)} ,$$

where n_F is a cutoff in n imposed by possible electric field ionization,

$$n_F = \{3.2\times 10^8\ [\mathrm{F(V/cm)}]^{-1}\}^{1/4} .$$

TABLE VI. Cross-section sums for C^{1+}, O^{3+}, Ar^{13+}, and Fe^{21+} and for the ground states $^2\bar{P}$ and $^4\bar{P}$, in units of 10^{-18} cm^2 and $\Delta e_c = 0.005$, 0.01, 0.05, and 0.1 Ry, respectively. n_g are the lowest n values allowed by energy conservation for the intermediate states d, and n_s are the lowest n values where all the allowed Auger channels are open. $l_{\max}$ is approximately determined as the highest l that contributes to the total DR, and is useful in estimating the field-enhancement effect.

	C^{1+}	O^{3+}	Ar^{13+}	Fe^{21+}
$\sum(^2\bar{P})$	24.6	38.7	16.7	11.8
$\sum(^4\bar{P})$	3.71	3.99	0.656	0.735
$l_{\max}$	4	6	10	11
n_g	3	5	12	12
n_s	9	13	20	23

A good agreement between theory and experiment of Dittner *et al.*[5] was obtained when $r_F \sim 2$ was used, which was below the estimated maximum r_F. On the other hand, the earlier C^{1+} case[3] is quite uncertain, and it would be of interest to test this by a new experiment. We note some of the general features of the cross sections. As Z_c increases, some of the radiative transitions involving HRS electrons (nl) become relatively more important. In addition, $l_{\max}$ steadily increases with Z_c. The fluorescence yields are small, typically $\omega \lesssim 10^{-3}$, and increase with n, like n^3. This of course makes σ^{DR} nearly constant in n, until n reaches either n_F or $n_c \sim [(f+b)/a]^{1/3}$, whichever is smaller. Contributions to the total DR cross section and rates from the $\Delta n_t \neq 0$ mode ($2s$ and $2p$ electron excitations to the M and N shells) are also being estimated.[12]

We have also estimated the cross section for the metastable initial state ^4P. Table VI summarizes the cross-section sums for the ground and metastable initial states.

The rate coefficients are compared with that given by Badnell;[13] α^{DR} for Fe^{21+} was estimated in Ref. 13 using the Burgess phenomenological formula, which is roughly 50% higher than our result. Recently reported values[13] of α^{DR} are in fair agreement with the present calculation. We present in Table VII the total rate coefficients α^{DR} for

TABLE VII. Total rate α^{DR} in units of 10^{-11} cm^3/sec for O^{3+} and C^{1+}. The unit of temperature is in Ry.

	$K_B T_e$	^4P	^2D	^2S	^2P	Sum
O^{3+}	0.3	0.0548	0.606	0.0498	0.238	0.949
	0.5	0.0430	1.25	0.161	0.919	2.37
	0.9	0.0256	1.41	0.575	1.94	3.95
	1.3	0.0170	1.19	0.511	1.88	3.60
	1.5	0.0143	1.08	0.470	1.78	3.34
C^{1+}	0.2	0.0010	0.340	0.0214	0.117	0.479
	0.6	0.0007	0.617	0.0811	0.642	1.34
	1.0	0.0	0.449	0.0663	0.579	1.09
	1.4	0.0	0.328	0.0511	0.464	0.843

C^{1+} and O^{3+} for each ^4P, ^2D, ^2S, and ^2P at different temperatures.

A smooth variation within the isonuclear sequences for the ions O, Ar, and Fe for $N=3$, 4, and 5 is found. This is shown in Fig. 4 for the ions (O^{3+}, O^{4+}, and O^{5+}), (Ar^{13+}, Ar^{14+}, and Ar^{15+}), and (Fe^{21+}, Fe^{22+}, and Fe^{23+}) where our data are compared with those of McLaughlin *et al.*[14]

In Table VIII we summarize all the relevant information for a sample calculation for the intermediate states $1s^2 2s 2p^2[^2P]13p, 13d$ for O^{3+}, where A_{a_1} is the Auger transition probability from the intermediate state to the initial state i and A_{a_2}, A_{a_3}, and A_{a_4} are those to $i'=^4P$, ^2D, and ^2S, respectively. A_{r_1} is the radiative transition probability for $^2P \rightarrow {}^2\bar{P}$ and A_{r_2} is the sum of the rest of the radiative transition probabilities. The cross sections σ^{DR} are given in units of 10^{-20} cm^2.

IV. CONCLUSION

The DR cross sections and rate coefficients are presented for ionic targets of the B-isoelectronic sequence at low energies, where only the $\Delta n_t=0$ ($2s \rightarrow 2p$) excitation mode is included. Other excitation modes ($\Delta n_t \neq 0$) at higher energies are not treated here; they are important in the evaluation of the total DR rate coefficients, especially at higher temperatures. This will be the subject of a future communication.[12] In the present study we neglected the effect of the plasma environment in which the DR process may take place, i.e., the field and density effects, as well as a possible nonequilibrium effect. The $\Delta n_t=0$ mode is especially sensitive to these perturbations and the rate coefficients should eventually be modified to incorporate them.

ACKNOWLEDGMENTS

The work reported here was supported in part by a U.S. Department of Energy grant. We benefited from several stimulating conversations with Dr. P. Dittner and Dr. S. Datz concerning the Oak Ridge National Laboratory experiment. Dr. I. Nasser was involved in the cross-section calculation of the O^{3+} case and was helpful during the initial stage of this work. We also thank Dr. R. Cowan for the use of his code RCN/RCG and for helpful discussions concerning the code. H. H. Ramadan was supported by the Egyptian channeling program.

APPENDIX: CONTRIBUTION OF HIGH RYDBERG STATES

We consider here an improvement of the procedure for estimating the contribution of high Rydberg states with large n to the total α^{DR} and σ^{DR}. This is especially important in the case of the $\Delta n_t=0$ mode. The lowest n value allowed for the process (1) is determined by energy conservation. Explicit calculation of $\bar{\sigma}^{DR}$ for each suc-

TABLE VIII. Cross section σ^{DR} for the intermediate states $1s^2 2s 2p^2[^2P]13p, 13d$, of O^{2+}, where $A_{r_{1,2,3,4}}$ are the Auger transitions from the intermediate state to $[^2P]$ initial state i and to ^4P, ^2D, and ^2S, respectively. $A_{r_{1,2}}$ are the radiative transitions for $^2P \rightarrow {}^2\bar{P}$ and the sum of the rest of the radiative transitions, respectively. σ^{DR} are given in units of 10^{-20} cm^2, and $\Delta e_c = 0.01\mathcal{R}$.

L	S	A_{a_1}	A_{a_2}	A_{a_3}	A_{a_4}	A_{r_1}	A_{r_2}	ω	σ^{DR}
1	0	0.373[+13]		0.552[+13]	0.221[+13]	0.105[+11]	0.116[+9]	0.923[−3]	0.147
1	1	0.127[+13]	0.578[+13]	0.618[+12]	0.245[+12]	0.105[+11]		0.384[−2]	0.626
2	0	0.329[+11]		0.612[+13]		0.105[+11]	0.116[+9]	0.172[−2]	0.004 02
2	1	0.582[+11]	0.302[+12]	0.685[+12]		0.105[+11]		0.992[−2]	0.123
1	0	0.846[+11]		0.161[+13]		0.105[+11]	0.100[+9]	0.622[−2]	0.0222
1	1	0.787[+11]	0.909[+12]	0.178[+12]		0.105[+11]	0.233[+9]	0.910[−2]	0.0908
2	0	0.820[+13]		0.222[+12]	0.145[+13]	0.105[+11]	0.226[+9]	0.108[−2]	0.753
2	1	0.158[+13]	0.205[+12]	0.247[+11]	0.160[+12]	0.105[+11]	0.251[+8]	0.531[−2]	1.77
3	0	0.954[+13]		0.434[+13]		0.105[+11]	0.226[+9]	0.770[−3]	1.05
3	1	0.205[+13]	0.510[+11]	0.482[+12]		0.105[+11]	0.251[+8]	0.405[−2]	2.45

cessive principal quantum number is carried out for each n until $\Gamma_a(d)$ attain the proper n^{-3} behavior, say, for $n \gtrsim n_m$. The rest of the HRS contribution to the rate is then calculated by integrating over n from n_m to infinity. It is important to make sure that no new Auger channels are open at $n \geq n_m$, i.e., $n_m \geq n_g$. Thus, for $n > n_m$, we have in general

$$\Gamma_r(d) = a + b/n^3 ,$$
$$\Gamma_a(d) = f + g/n^3 , \tag{A1}$$

where a and f are those radiative and Auger transition probabilities that do not depend upon n. The constants b and g represent the contributions to the width that directly involve the HRS electron. They are obtained from the A_r and A_a which are explicitly calculated at $n = n_m$. The fluorescence yield $\omega(d)$ is then parametrized as

$$\omega(d) = \Gamma_r/(\Gamma_r + \Gamma_a) \sim n^3 \left[\frac{1 + (b/a)n^{-3}}{\left[\frac{b+g}{a}\right] + \left[\frac{f+a}{a}\right] n^3} \right] . \tag{A2}$$

(Here, the distinction between Γ_r and Γ_r' is omitted for simplicity; Γ_r' retains only those A_r which lead to Auger stable final states.) In general, $(b+g)/a$ is very large, so that $\omega(d)$ will increase like n^3 until n reaches the value

$$n \sim n_c = \left[\frac{b+g}{a+f} \right]^{1/3} .$$

For $n > n_c$, $\omega(d)$ levels off and approaches the constant $a/(a+f)$, and hence $\sigma^{\mathrm{DR}}(n)$ starts to decrease like n^{-3}.

The cross section is constructed as

$$\bar{\sigma}^{\mathrm{DR}}(n) = \bar{\sigma}_0^{\mathrm{DR}} n^{-3} \left[\frac{a + b/n^3}{(a+f) + (b+g)/n^3} \right] , \tag{A3}$$

where

$$\bar{\sigma}_0^{\mathrm{DR}} = (2.68 \times 10^{-32}) V_a(n = n_m) n_m^3 \left[\frac{\mathcal{R}^2}{e_c \Delta e_c} \right]_{n_m} .$$

In (A3) we neglected the variation of e_c on n. This is reasonable for $n_m \gtrsim 20$, but can sometimes grossly overestimate the HRS contributions to σ and α when $n_m \lesssim 10$, by as much as a factor of 2 in some cases. In this appendix we attempt to improve the previous extrapolation formula[2] by incorporating the variation of e_c in n. The total Rydberg state contribution is defined as

$$\sum(i) \equiv \sum_{n=n_m}^{\infty} \bar{\sigma}^{\mathrm{DR}}(n) .$$

From (A3) the total contribution is given by

$$\sum_{n=n_m}^{\infty} \bar{\sigma}^{\mathrm{DR}}(n) = \bar{\sigma}_0^{\mathrm{DR}} \sum_{n=n_m}^{\infty} \frac{1}{n^3} \left[\frac{a + b/n^3}{(a+f) + (b+g)/n^3} \right] . \tag{A4}$$

Replacing the summation on the right-hand side by an integral, we get[2]

$$\sum_{n=n_m}^{\infty} \frac{1}{n^3} \left[\frac{a + b/n^3}{(a+f) + (b+g)/n^3} \right] \sim \frac{b}{2(b+g)} \frac{1}{n_c^2 x_m^2} + n_c \left[\frac{a}{b+g} - b\frac{(a+f)}{(b+g)^2} \right] F_A(x_m) , \tag{A4a}$$

where

$$F_A(x_m) = \frac{1}{3} \left[\frac{1}{2} \ln \left[\frac{x_m^2 - x_m + 1}{(x_m + 1)^2} \right] + \frac{\sqrt{3}\pi}{2} - \sqrt{3} \tan^{-1} \left[\frac{2x_m - 1}{\sqrt{3}} \right] \right] , \quad x_m \equiv \frac{n_m - \frac{1}{2}}{n_c} , \quad n_c = \left[\frac{b+g}{a+f} \right]^{1/3} .$$

When $x_m \leq 0.5$, $F_A(x_m) \sim 1.21 - x_m$ is a good approximation.

Since, in (A3), the variation of e_c with n is neglected, the total Rydberg state, evaluated using (A4a), overestimates the HRS contribution. An improved value is obtained by replacing $e_c(n_m)$ in (A3) by $\bar{e}_c$, where

$$\bar{e}_c = e_{cg} - \frac{Z^2}{\bar{n}^2} , \tag{A5}$$

with

$$e_{cg} = e_c(n = n_m) + \frac{Z^2}{n_m^2}, \quad \bar{n}^2 = n_c n_m + \frac{Z^2}{e_{cg}} \text{ for } \sigma^{\mathrm{DR}}, \quad \bar{n}^2 = n_c n_m + \frac{Z^2}{K_B T_e} \text{ for } \alpha^{\mathrm{DR}} .$$

Table IX contains two examples of a test calculation in which three different procedures are adopted: (i) exact explicit

TABLE IX. Comparison between the cross-section sums and rates obtained using the exact, old formula and improved extrapolation formulas for the intermediate states $1s^2 2s 2p^2[^2P]ns$ of O^{3+}, with $S=0$ (unprimed) and $S=1$ (primed). $k_B T_e = 1$ Ry, σ is in cm^2 and α in cm^3/sec, and $\Delta e_c = 0.01$ Ry.

	Exact	Old	Improved
$\sum \bar{\sigma}^{\mathrm{DR}}$	49.2[−20]	52.1[−20]	50.4[−20]
$\sum \bar{\sigma}^{\mathrm{DR}'}$	1.39[−18]	1.45[−18]	1.42[−18]
α^{DR}	0.391[−12]	0.420[−12]	0.400[−12]
α'^{DR}	0.110[−11]	0.117[−11]	0.113[−11]

term-by-term sum over n, (ii) the previous formula (A4a), and (iii) the improved formula using (A5) in (A3). Two intermediate states $1s^2 2s 2p^2[^2P]ns$ of O^{3+} with $S=0$ and 1 are chosen. Obviously, $\bar{e}_c = e_c$ $(n = n_m)$ gives an upper bound on the HRS contribution to $\bar{\sigma}$ and α, while $\bar{e}_c = e_{cg}$ gives a lower bound.

Finally, for a crude estimate, a simple empirical formula for the HRS contribution can be given:

$$\sum \approx \bar{\sigma}^{\mathrm{DR}}(n_m - 1)\left[\frac{n_m}{2}\right]\left[\frac{n_m - 1}{n_m}\right]^3\left[1+\frac{1}{n_m}+\frac{1}{2n_m}\right]\Big/\sqrt{\omega(n_m)}\ ,$$

which is proven to be very effective (to $\sim 20\%$ accuracy).

---

*Permanent address: Physics Department, Ain Shams University, Cairo, Egypt.

[1]Y. Hahn, Comments At. Mol. Phys. **19**, 99 (1987).
[2]Y. Hahn, Adv. At. Mol. Phys. **21**, 123 (1985).
[3]B. A. Mitchell *et al.*, Phys. Rev. Lett. **50**, 335 (1983).
[4]K. LaGattuta and Y. Hahn, Phys. Rev. Lett. **50**, 668 (1983).
[5]P. Dittner, S. Datz, R. Hippler, H. F. Krause, P. D. Miller, P. L. Pepmiller, C. M. Fou, Y. Hahn, and I. Nasser, Phys. Rev. A **38**, 2762 (1988).
[6]K. LaGattuta and Y. Hahn, Phys. Rev. Lett. **51**, 558 (1983); K. LaGattuta, I. Nasser, and Y. Hahn, Phys. Rev. A **33**, 2782 (1986); C. Bottcher, D. Griffin, and M. Pindzola, *ibid.* **34**, 860 (1986).
[7]I. I. Sobelman, *Introduction to the Theory of Atomic Spectra* (Pergamon, Oxford, 1972).
[8]A. Burgess, Mem. R. Astron. Soc. **69**, 1 (1964).
[9]R. D. Cowan (private communication).
[10]S. Bashkin and J. O. Stoner, Jr., in *Atomic Energy Levels and Grotrian Diagrams* (North-Holland, Amsterdam, 1975).
[11]Y. Hahn, K. LaGattuta, and I. Nasser, in *Atomic Excitation and Recombination in External Fields*, edited by M. H. Nayfeh and C. W. Clark (Harwood Academic, New York, 1985).
[12]M. Janjusevic and Y. Hahn (unpublished).
[13]N. R. Badnell, J. Phys. B **19**, 3827 (1986); N. R. Badnell and M. Pindzola (unpublished).
[14]D. J. McLaughlin and Y. Hahn, Phys. Rev. A **29**, 712 (1983); D. J. McLaughlin, K. J. LaGattuta, and Y. Hahn, J. Quant. Spectrosc. Radiat. Transfer **37**, 47 (1987).